THE JOURNAL OF PHYSICAL CHEMISTRY C

Article

pubs.acs.org/JPCC

Surface Effects on Structural Phase Transformations in Nanosized Shape Memory Alloys

Zhen Zhang,*[,†] Xiangdong Ding,[†] Junkai Deng,[†] Jian Cui,[†] Jun Sun,[†] Tetsuro Suzuki,[‡] Kazuhiro Otsuka,[‡] and Xiaobing Ren*[,†,‡]

[†]Multi-Disciplinary Materials Research Center, Frontier Institute of Science and Technology, State Key Laboratory for Mechanical Behavior of Materials, Xi'an Jiaotong University, Xi'an 710049, China

[‡]Ferroic Physics Group, National Institute for Materials Science, 1-2-1 Sengen, Tsukuba, 305-0047, Ibaraki, Japan

ABSTRACT: We systematically investigated the role of surface on the B2−B19 transformation of free-standing nanoparticles by classical molecular dynamics simulations. It was found that the surface of particles has a shell structure with a thickness of 2 unit cells, suppressing the B2−B19 transformation locally. Below a critical size, this surface shell leads to the reduction of the transformation latent heat and the vanishing of B2−B19 transformation. We propose a Landau-type model based on the core−shell structure of particles, which reproduces well the relation between transformation temperature and particle size. Our results provide a microscopic insight into the origin of surface-induced size effect on the structural phase transformations in nanosized shape memory alloys.

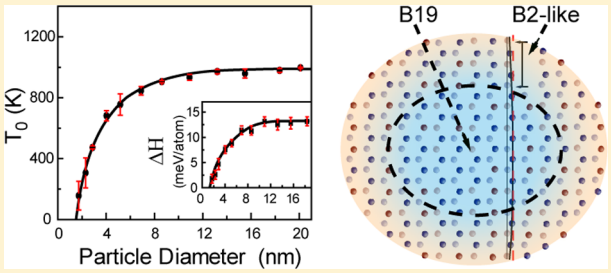

1. INTRODUCTION

A structural phase transformation enables shape memory alloys (SMAs) to exhibit fascinating properties such as shape memory effect and superelasticity.[1] Based on their unique properties, SMAs have been widely used in sensors, actuators, medical devices, and other applications. Recently, due to the requirement of micro/nano devices on their components to exhibit certain functionalities, transformations of micro/nanoscale materials have attracted significant interest.[2−6] Previous studies demonstrate that SMAs exhibit even better properties at small scale than their bulk counterparts, as manifested by the two-way shape memory effect in Cu−Al−Ni thin films, high damping capacity in Cu−Al−Ni pillars, and superelasticity with small hysteresis in Ti−Ni nanograins.[7−9]

Although SMAs exhibit promising properties at small scales, it was reported that their structural phase transformation disappears when the system size is further reduced to a critical value (typically a few nanometers). Simultaneously, the transformation latent heat drops dramatically. Such a size effect is found in a variety of important SMAs (e.g., Au−Cd,[10] Ti−Ni,[11] and Fe−Pd[12]), and it limits the further application of SMAs at nanoscale. Thus, understanding the size effect on structural phase transformations and predicting the critical size become important issues for nanosized SMAs.

Previous results indicate that external constraints such as the mismatch strain,[13] the oxidation or amorphous surface layer,[14,15] and the grain or phase boundary[11,16] can suppress the structural phase transformations of nanosized SMAs. However, external constraints are incapable of explaining the size effect on transformations of nearly free-standing Au−Cd nanoparticles[10] and oxidation-resistant Fe−Pt nanoparticles,[12] where external constraints are experimentally eliminated through a free surface. For these free-standing SMAs, it was assumed that their size effect is due to the dominance of surface relative to volume in nanocrystals. However, the microscopic nature of surface effect on structural phase transformations is unknown as yet. As a result, the relation between the large ratio of surface area (to volume) and the observed size effect on structural phase transformations has not been elucidated clearly. A model that relies on the microscopic nature of surface effect is still missing for the nanosized SMAs.

In the present paper, the B2−B19 transformation, possessed by many important SMAs, is investigated in free-standing nanoparticles in detail, aiming to achieve an atomic-level understanding of the surface effect. Moreover, the uncovering on the microscopic nature of surface effect will enable a clear microscopic picture and a Landau-type model of the surface-induced size effect on structural phase transformations in nanosized SMAs.

2. SIMULATION METHODS

Free-standing nanoparticles with diameter from 1.15 to 20 nm were studied by classical molecular dynamics simulations with a model alloy, the EAM potential of which was developed by Voter-Chen[17] and Farkas et al.[18] Lazarev et al. reported that this model alloy was able to reproduce the essential features of thermally induced B2−B19 transformation in bulk materials.[19] The particles were initialized as B2 structure, with 18%

Received: January 5, 2013
Revised: March 24, 2013
Published: March 25, 2013

substitutional defects introduced randomly (i.e., $A_{68}B_{32}$). The lattice constant of B2 structure was 2.87 Å. In order to eliminate the effect of external constraints and crystallographic orientation on structural phase transformations at nanoscale, free surface boundary condition was utilized.

The structural phase transformations of particles were studied by cooling and heating the system with Nose-Hoover thermostat.[20,21] To begin with, the particles were annealed in the parent phase for 50−100 ps to eliminate the as-built stress. Then, they were cooled to trigger the forward transformation (B2→B19). Finally, the particles were heated up to realize the reverse transformation (B19→B2). The cooling/heating rate was kept as 3.33 K/ps, which is a reasonable value in such studies.[22] The computer simulations were performed using the LAMMPS code.[23]

3. RESULTS

3.1. B2−B19 Transformation of Large Particles. The structural phase transformation of a large particle with diameter D = 18.4 nm is shown in Figure 1. Figure 1a shows that the potential energy drops steeply in a temperature interval below $M_s \sim 530$ K upon cooling. Within this temperature interval, as shown in Figures 1b1−b4, the fraction of low-temperature phase in the particle increases with cooling, indicating the forward transformation. As shown in Figures 1c1,c2, this particle transforms into B19 martensite phase, characterized by $\{110\}\langle\bar{1}10\rangle_P$ (P represents the B2 parent phase) basal plane shuffles.[24,25] Upon heating, Figure 1a shows that the potential energy appears to rise in a temperature interval near $A_f \sim 1350$ K, indicating the occurrence of a reverse transformation. Above 1350 K, Figures 1d1,d2 demonstrate that the B2 parent phase is restored. The potential energy curve of the particle with smaller size (D = 4.02 nm, shown in Figure 2a) exhibits similar behavior upon cooling and heating. The temperature intervals near M_s and A_f on cooling and heating curves indicate the occurrence of B2→B19 and B19→B2 transformations. As a result, a reversible B2−B19 transformation, similar to that of bulk materials, is reproduced by the present model alloy with a large particle size.

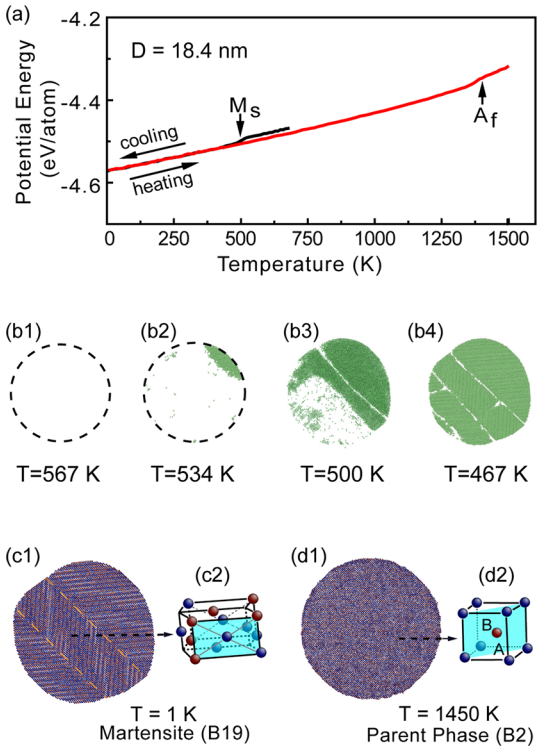

Figure 1. B2−B19 transformation of a large particle with diameter D = 18.4 nm. (a) Potential energy as a function of temperature. (b1)−(b4) The martensite phase (green) in the particle at 567 K ($T > M_s$), 534 K ($T < M_s$), 500 K, and 467 K respectively. (c1) and (c2) Morphology and local structure of the particle at 1 K. (d1) and (d2) Morphology and local structure of the particle at 1450 K. Coloring represents atom type: blue, A atoms; red, B atoms.

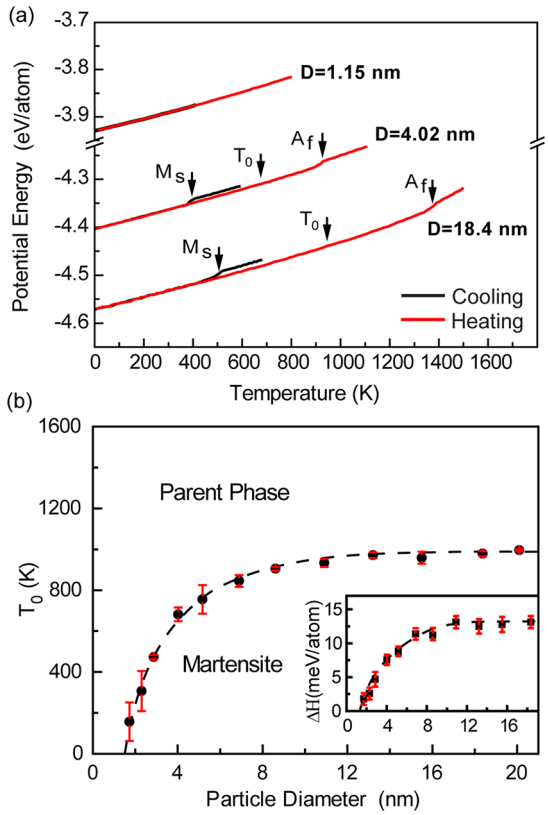

Figure 2. Size effect associated with the B2−B19 transformation of free-standing nanoparticles. (a) Potential energy curves of particles with the diameter D = 1.15, 4.02, and 18.4 nm. (b) Transformation temperature T_0 as a function of particle diameter, where $T_0 = (M_s + A_f)/2$. Inset shows the relation between transformation latent heat ΔH and particle size. Error bars show the standard deviation of T_0 and ΔH at each diameter.

3.2. Size Effect of B2−B19 Transformation. Figure 2a shows potential energy curves of three typical particles, ranging from 18.4 to 1.15 nm in diameter. With reducing the particle size from D = 18.4 nm to D = 4.02 nm, the transformation temperatures (both M_s and A_f) decrease. Moreover, the transformation hysteresis (i.e., the temperature difference $A_f - M_s$) becomes smaller with reducing size, being consistent with experimental observations on Au−Cd nanoparticles.[26] When the particle size decreases to 1.15 nm, the transformation disappears. It is thus demonstrated that the B2−B19 transformation within the present model alloy has strong dependence on size.

Figure 2b shows the relation between transformation temperature T_0 and particle size quantitatively, where $T_0 = (M_s + A_f)/2$. When the particle diameter is larger than 14 nm,

dx.doi.org/10.1021/jp401670r | J. Phys. Chem. C 2013, 117, 7895−7901

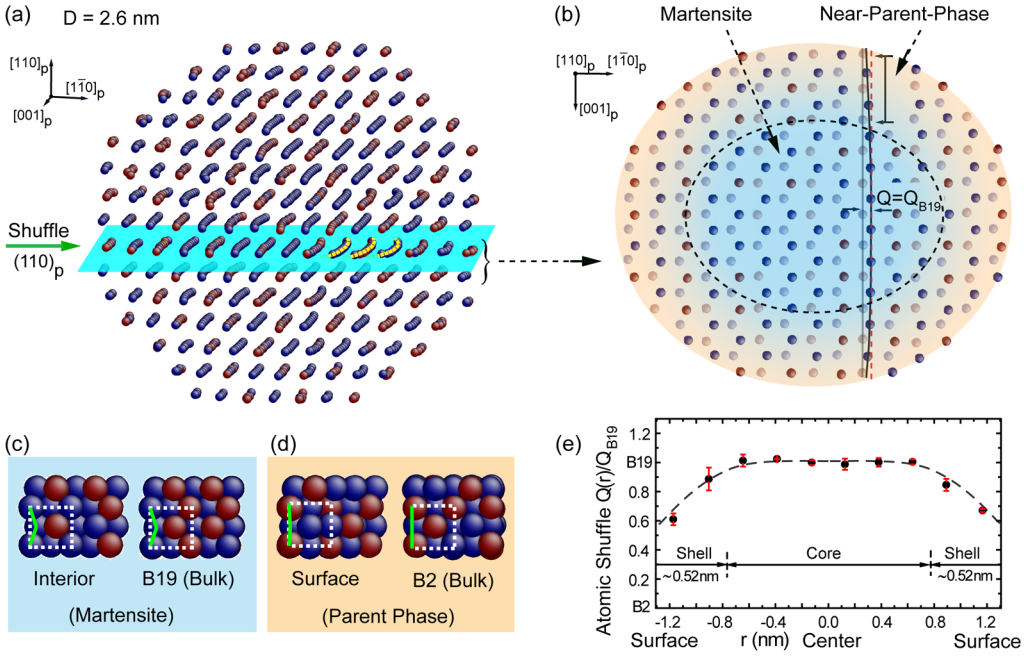

Figure 3. Core−shell structure of a martensite particle with the diameter D = 2.6 nm. (a) Structure of the martensite particle at 1 K. The nonuniform feature of martensite particle is indicated by curved yellow lines in $(110)_P$ basal plane. (b) The atomic shuffle between two neighboring $(110)_P$ planes. The dashed circle indicates the border between the martensite core and the near-parent-phase shell. The deviation between the vertical gray line and black line indicates the atomic shuffle along $[1\bar{1}0]_P$. (c) Comparison of the structure between particle's interior and B19 martensite. (d) Comparison of the structure between particle's surface and B2 parent phase. (e) Spatial distribution of normalized atomic shuffles in this martensite particle. The standard deviation of atomic shuffles is shown by error bars.

T_0 is independent of particle size. When the particle diameter becomes smaller than 14 nm, T_0 begins to decrease. Eventually, the B2−B19 transformation disappears when the particle diameter is smaller than 1.15 nm. The latent heat, deduced from the drop of potential energy at M_s temperature and plotted in the inset of Figure 2b, also exhibits the size effect. It is found that the latent heat gradually decreases with reducing size. When the particle size reaches 1.15 nm, latent heat drops to zero.

Our simulation results are consistent with the experimental observations. Many important SMAs, such as Au−Cd alloys[27] and Ti−Ni based alloys,[24] possess the B2−B19 transformation. Moreover, the transformation temperature and transformation latent heat of these alloys are found to decrease with reducing particle size.[26]

3.3. Microscopic Nature of the Surface Effect. Previous results show that the B2−B19 transformation is characterized by the appearance of long-range-ordered atomic shuffles in B19 martensite phase.[27,28] Thus, we study the distribution of atomic shuffles being close and far away from the surface in martensite particles to reveal the microscopic nature of surface effect on the B2−B19 transformation.

A martensite particle with diameter of 2.6 nm is shown in Figure 3a. Interestingly, the arrangement of atoms in the $(110)_P$ basal plane of this particle is nonuniform and exhibits deviation near surface. In order to reveal this feature clearly, two neighboring $(110)_P$ planes are cut from the particle and shown in Figure 3b. It is found that these two planes shuffle relatively along $[1\bar{1}0]_P$ direction. We indicate the atomic shuffle between two planes by a splitting between gray and black lines. It is found that the nonuniform feature of atomic shuffles is characterized by a border (indicated by the dashed circle), separating the particle into core and shell.

As Figure 3c shows, the structure of the core region of this particle is identical to the B19 phase of bulk materials. However, Figure 3d shows that the structure of surface shell is close to the parent phase, where the atomic shuffles in $(110)_P$ planes nearly vanish. Quantitative results on the spatial distribution of atomic shuffles of this particle in Figure 3e show that the thickness of this shell is ~0.52 nm (almost two unit cells).

Furthermore, we show the surface effect of B2−B19 transformation with the particle diameters D = 1.7, 8.61, and 18.4 nm in Figures 4a−c. It is found that although there is a large variation in size, all these martensite particles possess a surface shell, where the atomic shuffles deviate from that of the B19 core region and approach the B2 parent phase. The existence of this surface shell in particles is further demonstrated by quantitative results on the thickness of near-parent-phase shell in martensite particles (Figure 4d).

The reported experimental results on SMA nanoparticles also suggest the inhomogeneity of martensite phase near surface. TEM images of nearly free-standing Au−Cd nanoparticles show that some particles contain martensite phase in the core region and parent phase near surface,[10] being consistent with the core−shell structure of martensite particles of the present model alloy. These results demonstrate that the surface of SMA particles is actually a shell with certain thickness, which locally suppresses the structural phase transformation.

4. DISCUSSION

4.1. Explanation of Shell Structure of Martensite Particles. We explain the structure of the surface shell of martensite particles based on the energy variation of this shell during the B2−B19 transformation. The total potential energy of the particle (E) is divided into shell energy and bulk energy.

dx.doi.org/10.1021/jp401670r | J. Phys. Chem. C 2013, 117, 7895−7901

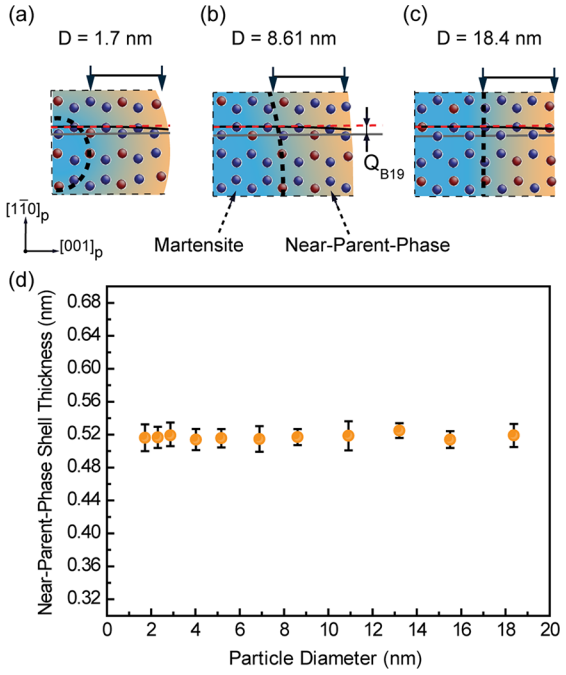

Figure 4. (a, b, c) Atomic shuffle between two neighboring $(110)_P$ planes near the surface of martensite particles with the diameter D = 1.7, 8.61, and 18.4 nm, respectively. (d) Thickness of the near-parent-phase shell in martensite particles. The standard deviation of shell thickness is shown by error bars.

The bulk energy is defined as N_aE_c, where N_a is the number of atoms in the particle and E_c is the average potential energy of atoms in the core region. Therefore, the bulk energy can represent the energy variation of the particle during the transformation without considering the surface shell. The shell energy is calculated as $E - N_aE_c$. Consequently, the shell energy of martensite particle here includes both the excess energy due to surface and the gradient energy due to the variation of atomic shuffles in the surface shell.

We take a particle with D = 8.61 nm as an example to demonstrate the variation of shell energy and bulk energy during the B2−B19 transformation. As Figure 5 shows, the B2 → B19 transformation reduces the bulk energy at M_s temperature. However, the B2 → B19 transformation increases the shell energy at M_s temperature. This result demonstrates

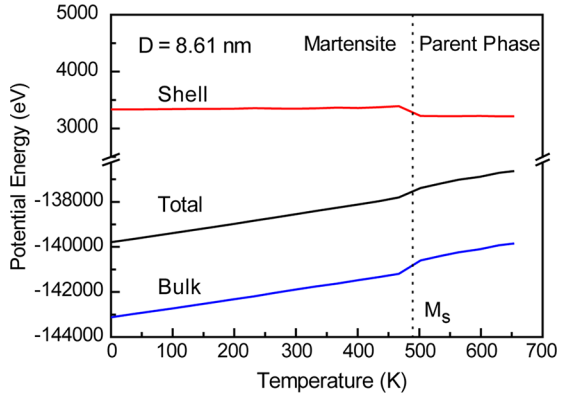

Figure 5. Variation of total potential energy, shell energy, and bulk energy during the B2−B19 transformation of a particle with the diameter D = 8.61 nm.

that the B2 → B19 transformation is energetically favored by the core region but disfavored by the surface shell. As a result, the structure of the surface shell deviates from that of the B19 core and approaches the B2 parent phase. This microscopic feature of the surface shell of martensite particles is analogous to the appearance of surface relaxation in ferroelectric $BaTiO_3$ and $PbTiO_3$ nanoparticles,[29] surface spin disorder in ferrimagnet γ-Fe_2O_3 nanoparticles,[30] and surface elastic anomaly of nanomaterials where anharmonicity coming from the competition between springs is considered.[31,32]

4.2. Microscopic Explanation of the Disappearance of Structural Phase Transformation. We propose a schematic picture, as shown in Figure 6a, based on the existence of surface

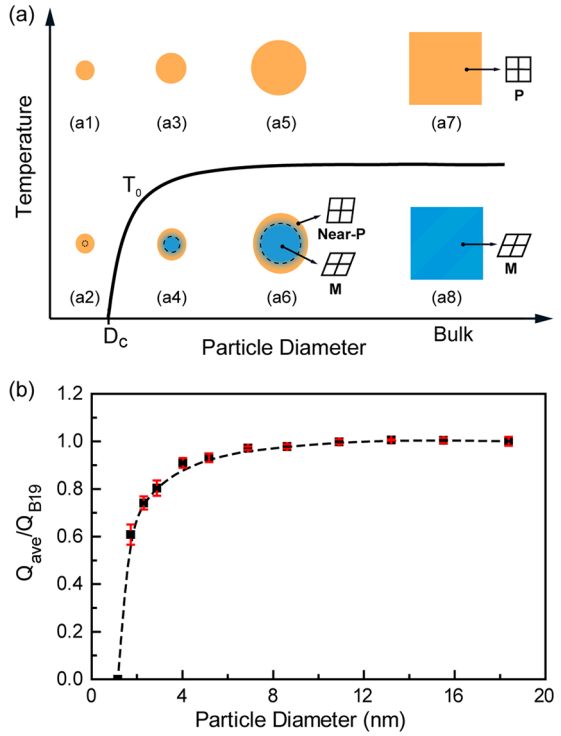

Figure 6. (a) Microscopic picture of the surface-induced size effect on structural phase transformation of free-standing nanoparticles. T_0 is the transformation temperature. D_c is the critical size below which transformation vanishes. [(a1) and (a2)], [(a3) and (a4)], and [(a5) and (a6)] High- and low-temperature phases of SMA nanoparticles with the diameter $D < D_c$, $D \sim D_c$, and $D > D_c$, respectively. (a7) and (a8) High- and low-temperature phase of bulk SMAs. The dashed line in (a2), (a4), and (a6) characterizes the surface shell, which favors the parent phase. P, M, and Near-P represent parent phase, martensite phase, and near-parent structure, respectively. (b) Average atomic shuffle of particles at 1 K as a function of particle size, normalized by the atomic shuffle of bulk B19 martensite. The standard deviation of atomic shuffle is shown by error bars.

shell, to explain microscopically the disappearance of structural phase transformation with reducing particle size. The parent phase and the martensite phase of bulk materials are shown in Figures 6a7,a8 as a reference. For nanosized SMAs, as Figure 6a shows, the ideal martensite phase cannot be reached. Instead, martensite particles are covered by a shell, the structure of which is close to the parent phase.

When the particle size is large, as shown in Figures 6a5,a6, the volume fraction of the surface shell in the whole particle is small. As a result, the phase transformation of large particles is

dx.doi.org/10.1021/jp401670r | J. Phys. Chem. C 2013, 117, 7895−7901

not affected by the surface shell. With reducing the particle size, as shown in Figures 6a3,a4, the volume fraction of the surface shell gradually increases. Then, the surface shell not only preserves parent phase therein but also leads to the vanishing of martensite phase of the whole particle. Consequently, the stability of particle with martensite phase reduces and the transformation temperature drops. Below the critical size, as shown in Figures 6a1,a2, the surface shell dominates the whole particle. As a result, the martensite phase is fully destabilized by the surface shell. The phase transformation disappears completely.

The microscopic picture is consistent with the simulation results. As shown in Figure 6b, the martensite phase of particles characterized by the average atomic shuffle is not affected by the surface shell when particle size is larger than 14 nm. Below 14 nm, the martensite phase of particles gradually diminishes, indicating the gradual dominance of surface shell. Simultaneously, as Figure 2b shows, the transformation temperature starts to decrease. Below 1.15 nm, the martensite phase of particles disappears, indicating the full destabilization of martensite phase.

4.3. Microscopic Explanation of the Reduction of the Transformation Latent Heat with Decreasing Particle Size. We further utilize the schematic picture (Figure 6a) to explain microscopically the decrease of the transformation latent heat with reducing particle size (Figure 2b inset). The latent heat of a structural phase transformation is proportional to the change of structure between the high- and low-temperature phase at the transformation temperature.[33] For bulk materials (Figures 6a7,a8), the transformation is between parent phase and fully transformed martensite phase; thus, the transformation latent heat is the largest. For nanoparticles, as shown in Figures 6a5,a6, the transformation is between parent phase and martensite phase covered by near-parent-phase shell; thus, the latent heat becomes smaller than that of bulk crystal in nanoparticles. Besides, the ratio of the shell region relative to the total volume increases with decreasing particle size. As a result, the latent heat decreases with decreasing particle size in nanoparticles. Therefore, the size effect of the latent heat is justified quite well by the present core−shell picture.

5. A MODEL

From simulation results, a B2-like surface shell is observed in martensite nanoparticles. The picture of core−shell structure is established and used to explain microscopically the disappearance of B2−B19 transformation at nanoscale. Experimentally, a similar size effect is also observed in other kinds of structural phase transformations.[10,12] Then it is possible that their size effect can be ascribed to the existence of the surface shell. Thus, by taking account of the surface shell, we propose a Landau-type model to study generally the disappearance of structural phase transformations at nanoscale.

5.1. Landau-Type Model of Structural Phase Transformation. The spatial distribution of order parameter in martensite particles is shown in Figure 7a. The extrapolation length δ (>0) is used as a phenomenological parameter to characterize the surface shell which favors the parent phase. In the present study, we assume the extrapolation length is independent of temperature and particle size.

For bulk materials, the Laudau free energy of structural phase transformations can be written as[34]

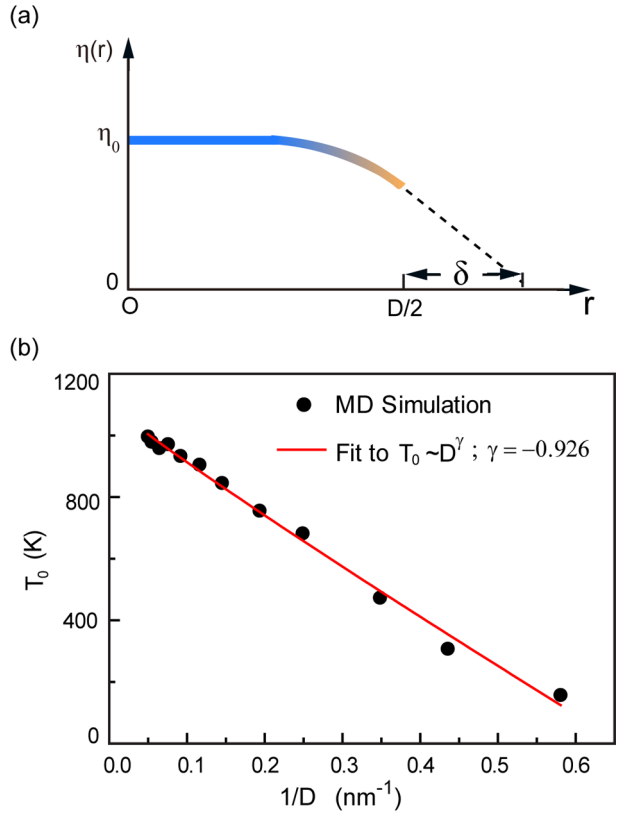

Figure 7. (a) Schematic diagram of the spatial distribution of order parameter η from the center O to the surface $D/2$ in martensite particles. The distance to the center of particles is represented by r. (b) The T_0 vs $1/D$ curve for simulation results, fitted by the $T_0 \sim D^{\gamma}$ relation where γ is found to be −0.926.

$$F = \frac{1}{2}A\eta^2 + \frac{1}{4}B\eta^4 + \frac{1}{6}C\eta^6 + \frac{1}{2}g(\nabla\eta)^2,$$
$$A = A_0(T - T_c^B) \quad (1)$$

where η is the order parameter; A_0 (>0), B (<0), and C (>0) are coefficients related to the SMA systems; g (>0) is the coefficient of gradient energy, which is introduced to characterize the gradient of order parameter in the surface shell. For first-order phase transformation, the transformation occurs at T_0^B in bulk materials, which is higher than T_c^B,[35] i.e.

$$T_0^B = T_c^B + 3B^2/16A_0C \quad (2)$$

In order to characterize the surface effect, a boundary condition is added corresponding to Figure 7a as

$$\nabla\eta|_{r=D/2} = -\frac{1}{\delta}\eta|_{r=D/2} \quad (3)$$

To deduce the relation between the transformation temperature T_0 and the particle diameter D, we minimize the free energy eq 1 with respect to η as

$$A\eta + B\eta^3 + C\eta^5 = g\nabla^2\eta, \quad A = A_0(T - T_c^B) \quad (4)$$

Interestingly, the Euler−Lagrange equation (eq 4) and surface condition (eq 3) of a structural phase transformation possess the same forms as those of a first-order ferroelectric transition.[36,37] With similar deduction processes, the relation between transformation temperature T_0 and particle diameter D can be obtained from eqs 3 and 4 as

dx.doi.org/10.1021/jp401670r | J. Phys. Chem. C 2013, 117, 7895−7901

$$T_0 = T_0^B - \frac{2g}{A_0\delta}D^{-1} \quad (5)$$

5.2. Comparison of Analytical Model with Simulation Results. Equation 5 shows that the transformation temperature T_0 decreases with reducing particle size D, following a $T_0 \sim D^{-1}$ relation. As Figure 7b shows, we fit the simulation results with the $T_0 \sim D^{\gamma}$ relation. The fitted exponent γ is −0.926, which is consistent with the deduced value (i.e., −1). Moreover, the $T_0 \sim D^{-1}$ relation for a structural phase transformation was also reported in Ti−Ni nanoparticles,[38] Fe−Ni nanoparticles,[39] and Fe nanowires,[22] thus implying the universality of the surface-induced size effect on structural phase transformations.

Based on the analytical model, the structural phase transformations of real SMAs at nanoscale and their critical sizes could be estimated since the parameters in the present model can be obtained from experiment. A_0, g, and T_0^B can be obtained from the transformation properties of bulk materials, and the extrapolation length δ can be measured directly from high-resolution TEM images.

Interestingly, the size effect also occurs for other phase transitions such as ferroelectric transitions[40] and ferromagnetic transitions,[41] and a similar core−shell structure is observed.[29,30,42] For ferroelectric and ferromagnetic systems, similar gradient energy terms and boundary conditions are added to the Landau free energy to describe their transitions at nanoscale phenomenologically.[43−45] Therefore, the present results suggest that there may be a generic microscopic feature of the surface-induced size effect for different kinds of transitions.

6. CONCLUSIONS

We have studied the microscopic nature of surface effect for the B2−B19 transformation of free-standing nanoparticles. Atomic level investigations of the structure of particles show that the surface of SMA nanoparticles has a certain thickness, i.e., a shell structure with 2 unit cells suppressing the transformation locally. Being dominant, this surface shell weakens the structural phase transformation of nanosized SMAs and results in the observed size effect. A solvable Landau-type model further confirms the temperature effect of such shell on structural phase transformation. We believe that the present study provides a solution to the long-standing puzzle of the surface-induced size effect on structural phase transformations and a quantitative model that can be used to predict the transformation properties of real SMAs in nanoscale.

AUTHOR INFORMATION

Corresponding Author

*E-mail: zhenn.zhang@gmail.com (Z.Z.); ren.xiaobing@nims.go.jp (X.B.R.).

Notes

The authors declare no competing financial interest.

ACKNOWLEDGMENTS

We thank A. Saxena for careful reading of the manuscript. The authors are grateful to Y. Ni, D. Xue, and Y. Wang for helpful discussions. The authors gratefully acknowledge the support of National Basic Research Program of China (2012CB619401, 2010CB613003), National Natural Science Foundation of China (51171140, 50831004 and 50771079), and 111 project of China (B06025).

REFERENCES

(1) Otsuka, K.; Wayman, C. M. *Shape Memory Materials*; Cambridge University Press: Cambridge, UK, 1998.
(2) Kahn, H.; Huff, M. A.; Heuer, A. H. The TiNi Shape-Memory Alloy and Its Applications for MEMS. *J. Micromech. Microeng.* **1998**, *8*, 213−221.
(3) Sutrakar, V. K.; Roy Mahapatra, D. Universal Stability and Temperature Dependent Phase Transformation in Group VIIIB−IB Transition Metal FCC Nanowires. *J. Phys. Chem. C* **2011**, *115*, 10394−10398.
(4) Li, S.; Ding, X.; Li, J.; Ren, X.; Sun, J.; Ma, E. High-efficiency Mechanical Energy Storage and Retrieval Using Interfaces in Nanowires. *Nano Lett.* **2010**, *10*, 1774−1779.
(5) Park, H. S.; Gall, K.; Zimmerman, J. A. Shape Memory and Pseudoelasticity in Metal Nanowires. *Phys. Rev. Lett.* **2005**, *95*, 255504.
(6) Saxena, A.; Aeppli, G. Phase Transitions at the Nanoscale in Functional Materials. *MRS Bull.* **2009**, *34*, 804−813.
(7) Bhattacharya, K.; James, R. D. The Material is the Machine. *Science* **2005**, *307*, 53−54.
(8) San Juan, J.; Nó, M. L.; Schuh, C. A. Nanoscale Shape-Memory Alloys for Ultrahigh Mechanical Damping. *Nat. Nanotechnol.* **2009**, *4*, 415−419.
(9) Tsuchiya, K.; Inuzuka, M.; Tomus, D.; Hosokawa, A.; Nakayama, H.; Morii, K.; Todaka, Y.; Umemoto, M. Martensitic Transformation in Nanostructured TiNi Shape Memory Alloy Formed via Severe Plastic Deformation. *Mater. Sci. Eng., A* **2006**, *438−440*, 643−648.
(10) Asaka, K.; Hirotsu, Y.; Tadaki, T. Structure of Nanometer-Sized Au-Cd Alloy Particles near Equiatomic Compositions at Room Temperature. *Mater. Sci. Eng., A* **2001**, *312*, 232−236.
(11) Waitz, T.; Kazykhanov, V.; Karnthaler, H. P. Martensitic Phase Transformations in Nanocrystalline NiTi Studied by TEM. *Acta Mater.* **2004**, *52*, 137−147.
(12) Seki, K.; Kura, H.; Sato, T.; Taniyama, T. Size Dependence of Martensite Transformation Temperature in Ferromagnetic Shape Memory Alloy FePd. *J. Appl. Phys.* **2008**, *103*, 063910.
(13) Roytburd, A. L.; Kim, T. S.; Su, Q.; Slutsker, J.; Wuttig, M. Martensitic Transformation in Constrained Films. *Acta Mater.* **1998**, *46*, 5095−5107.
(14) Fu, Y.; Shearwood, C. Characterization of Nanocrystalline TiNi Powder. *Scr. Mater.* **2004**, *50*, 319−323.
(15) Santamarta, R.; Schryvers, D. Effect of Amorphous-Crystalline Interfaces on the Martensitic Transformation in $Ti_{50}Ni_{25}Cu_{25}$. *Scr. Mater.* **2004**, *50*, 1423−1427.
(16) Lookman, T.; Littlewood, P. Nanoscale Heterogeneity in Functional Materials. *MRS Bull.* **2009**, *34*, 822−831.
(17) Voter, A. F.; Chen, S. P. Accurate Interatomic Potentials for Ni, Al and Ni_3Al. *Mater. Res. Soc. Proc.* **1987**, *82*, 175−180.
(18) Farkas, D.; Mutasa, B.; Vailhe, C.; Ternes, K. Interatomic Potentials for B2 NiAl and Martensitic Phases. *Model. Simul. Mater. Sci. Eng.* **1995**, *3*, 201−214.
(19) Lazarev, N. P.; Abromeit, C.; Schaublin, R.; Gotthardt, R. Temperature-Controlled Martensitic Phase Transformations in a Model NiAl Alloy. *J. Appl. Phys.* **2006**, *100*, 063520.
(20) Nose, S. A Unified Formulation of the Constant Temperature Molecular Dynamics Methods. *J. Chem. Phys.* **1984**, *81*, 511−519.
(21) Hoover, W. G. Canonical Dynamics: Equilibrium Phase-Space Distributions. *Phys. Rev. A* **1985**, *31*, 1695−1697.
(22) Sandoval, L.; Urbassek, H. M. Finite-Size Effects in Fe-Nanowire Solid-Solid Phase Transitions: A Molecular Dynamics Approach. *Nano Lett.* **2009**, *9*, 2290−2294.
(23) Plimpton, S. J. Fast Parallel Algorithms for Short-range Molecular Dynamics. *J. Comput. Phys.* **1995**, *117*, 1−19.
(24) Otsuka, K.; Ren, X. Physical Metallurgy of Ti-Ni-Based Shape Memory Alloys. *Prog. Mater. Sci.* **2005**, *50*, 511−678.
(25) Sanati, M.; Saxena, A.; Lookman, T.; Albers, R. C. Landau Free Energy for a bcc-hcp Reconstructive Phase Transformation. *Phys. Rev. B* **2001**, *63*, 224114.

(26) Frommen, C.; Wilde, G.; Rosner, H. Wet-chemical Synthesis and Martensitic Phase Transformation of Au-Cd nanoparticles with Near-Equiatomic Composition. *J. Alloys Compd.* **2004**, *377*, 232−242.
(27) Barsch, G. R.; Ohba, T.; Hatch, D. M. Landau Theory of Structural Transformations in Titanium-nickel and Gold-cadmium Alloys. *Mater. Sci. Eng., A* **1999**, *273*, 161−165.
(28) Khachaturyan, A. G. *Theory of Structural Transformation in Solid*; John Wiley & Sons: New York, 1983.
(29) Ishikawa, K.; Uemori, T. Surface Relaxation in Ferroelectric Perovskites. *Phys. Rev. B* **1999**, *60*, 11841−11845.
(30) Gazeau, F.; Bacri, J. C.; Gendron, F.; Perzynski, R.; Raikher, Y. L.; Stepanov, V. I.; Dubois, E. Magnetic Resonance of Ferrite Nanoparticles: Evidence of Surface Effects. *J. Magn. Magn. Mater.* **1998**, *186*, 175−187.
(31) Salje, E. K. H. A Pre-martensitic Elastic Anomaly in Nanomaterials: Elasticity of Surface and Interface Layers. *J. Phys.: Condens. Matter* **2008**, *20*, 485003.
(32) Houchmanzadeh, B.; Lajzerowicz, J.; Salje, E. K. H. Interfaces and Ripple States in Ferroelastic Crystals—A Simple Model. *Phase Transit.* **1992**, *38*, 77−87.
(33) Careri, G. *Order and Disorder in Matter*; Addison-Wesley: Reading, MA, 1984.
(34) Salje, E. K. H. *Phase Transitions in Ferroelastic and Co-elastic Crystals*; Cambridge University Press: Cambridge, UK, 1993.
(35) Krumhansl, J. A. Landau Models for Structural Phase Transitions: Are Soft Modes Needed? *Solid State Commun.* **1992**, *84*, 251−254.
(36) Tilley, D. R.; Žekš, B. Landau Theory of Phase Transitions in Thick Films. *Solid State Commun.* **1984**, *49*, 823−828.
(37) Bratkovsky, A. M.; Levanyuk, A. P. Smearing of Phase Transition Due to a Surface Effect or a Bulk Inhomogeneity in Ferroelectric Nanostructures. *Phys. Rev. Lett.* **2005**, *94*, 107601.
(38) Mutter, D.; Nielaba, P. Simulation of the Thermally Induced Austenitic Phase Transition in NiTi Nanoparticles. *Eur. Phys. J. B* **2011**, *84*, 109−113.
(39) Kadau, K.; Gruner, M.; Entel, P.; Kreth, M. Modeling Structural and Magnetic Phase Transitions in Iron-Nickel Nanoparticles. *Phase Transit.* **2003**, *76*, 355−366.
(40) Fong, D. D.; Stephenson, G. B.; Streiffer, S. K.; Eastman, J. A.; Auciello, O.; Fuoss, P. H.; Thompson, C. Ferroelectricity in Ultrathin Perovskite Films. *Science* **2004**, *304*, 1650−1653.
(41) Ambrose, T.; Chien, C. Finite-Size Effects and Uncompensated Magnetization in Thin Antiferromagnetic CoO Layers. *Phys. Rev. Lett.* **1996**, *76*, 1743−1746.
(42) Jia, C. L.; Nagarajan, V.; He, J. Q.; Houben, L.; Zhao, T.; Ramesh, R.; Urban, K.; Waser, R. Unit-Cell Scale Mapping of Ferroelectricity and Tetragonality in Epitaxial Ultrathin Ferroelectric Films. *Nat. Mater.* **2006**, *6*, 64−69.
(43) Ishibashi, Y.; Orihara, H.; Tilley, D. R. Thickness Transitions of Ferroelectricity in Thin Films. *J. Phys. Soc. Jpn.* **1998**, *67*, 3292−3297.
(44) Kaganov, M. I.; Omel'Yanchuk, A. N. Phenomenological Theory of Phase Transition in a Thin Ferromagnetic Plate. *Sov. Phys. JEPT* **1972**, *34*, 895−898.
(45) Zhong, W. L.; Wang, Y. G.; Zhang, P. L.; Qu, B. D. Phenomenological Study of the Size Effect on Phase Transitions in Ferroelectric Particles. *Phys. Rev. B* **1994**, *50*, 698−703.